Int. J. Electrochem. Sci., 15 **(2020)** 6815 – 6828, doi: 10.20964/2020.07.56

International Journal of
ELECTROCHEMICAL
SCIENCE
www.electrochemsci.org

High Performance of MWCNTs - Chitosan Modified Glassy Carbon Electrode for Voltammetric Trace Analysis of Cd(II)

J. Calvillo Solís, M. Galicia[*]

Universidad Autónoma de Ciudad Juárez, Departamento de Ciencias Químico-Biológicas, C.P. 32300, Juárez, CH. México.
[*]E-mail: monica.galicia@uacj.mx

Received: 3 March 2020 / *Accepted:* 22 April 2020 / *Published:* 10 June 2020

A scaffold of multiwalled carbon nanotubes (MWCNT) and chitosan biopolymer were assembled on glassy carbon electrode (GCE) for Cadmium(II) ion detection in aqueous solution. The electrodes were characterized using cyclic voltammetry and electrochemical impedance spectroscopy. Parameters for the electrochemical detection of cadmium ions were optimized using Square Wave Anodic Stripping Voltammetry (SWASV), with an acetate buffer at a pH of 5. A limit of detection of 0.09 μg L^{-1} was achieved. Moreover, detection selectivity was demonstrated using SWASV with this modified electrode for Cd(II) detection in the presence of other toxic heavy metal ions, including 30 μg L^{-1} Pb(II), 30 μg L^{-1} Co(II), and 100 μg L^{-1} Hg(II). This electrode combined with SWASV provides a new perspective for simultaneous detection of these species with a very low limit of detection.

Keywords: Anodic stripping voltammetry, glassy carbon electrode, MWCNTs, Trace analysis, Cd(II)

1. INTRODUCTION

Environmental pollution caused by heavy metals has been a major concern over the last 50 years, primarily due to the increasingly frequent presence of these pollutants in marine environments, agricultural soils, and air. Cadmium is one of the most dangerous heavy metals and is considered to damage both the human body and ecosystems. Exposure to this heavy metal generally arises from contaminated water intake, caused by the discharge of mining and industrial leaching, which is a primary route of contamination in water bodies [1]. In living organisms, cadmium causes severe health problems. For instance, high concentrations of cadmium generate physiological alterations, causing damage to tissue, cardiovascular system, central nervous system, and immune system. Furthermore, cadmium has been confirmed as a carcinogenic element [2].

Therefore, it is necessary to monitor and quantify this metal in very small concentrations,

preferably at the trace level. For this purpose, various analytical methods are currently used, such as atomic absorption spectroscopy [3], atomic fluorescence spectroscopy, [4] and, more recently, inductively coupled plasma mass spectroscopy [5]. However, these techniques have some disadvantages, such as the requirement for highly complex equipment representing high operating costs [6], time-consuming sample preparation procedures [7], and the necessity of a high level of knowledge for operation [8]. Fortunately, electrochemical methods offer an alternative approach for trace analysis of cadmium and other metals in solution [9-11].

Among the electroanalytical techniques employed, Square Wave Anodic Stripping Voltammetry (SWASV) offers high selectivity and low detection limits. This technique is based on the application of (stair case potential). In this process, the current is recorded for the anodic and cathodic potentials, and the difference between these two currents is the maximum current ($\Delta ip = ip_a - ip_c$), which is directly proportional to the concentration of the chemical species [12,13]. The results obtained from electroanalysis are straightforward, resulting in Gaussian bell-shaped peaks, with little distortion caused by the capacitive current [14]. Compared to other electroanalytical techniques such as Differential Pulse Anodic Stripping Voltammetry (DPASV) and Normal Pulse Voltammetry (NPV), SWASV is more sensitive and selective [15]. Additionally, voltammograms can be rapidly obtained, and the technique is relatively simple and low-cost [8,16].

An appropriate electroanalytical technique is essential for obtaining accurate and reliable results. However, the experimental setup is also a fundamental component of this technique; for example, modified glassy carbon electrodes allow to significantly improve the precision, detection limits, quantification, precision, accuracy, and reproducibility [17]. For this approach, various materials have been proposed, including polymers, metal/organometallic complexes, metal nanoparticles (M-NPs), organic molecules, and macromolecules [18]. However, carbon nanotubes (CNT) and their variants have emerged as one of the most versatile and efficient materials [19,20]. CNT are carbon allotropes with properties that are intermediate between those of graphite and fullerenes. CNT can be formed by sp_2-oriented carbon bonds and consist of a single layer [single-walled CNT (SWCNTs)] or multiple concentric tubes [multi-walled CNT (MWCNTs)] of rolled graphene, with a separation of approximately 0.35–0.40 nm [21]. CNT also exhibit a low production cost per unit [22], high thermochemical stability [23], remarkable surface activity [24], and chemical inertia [25]. Moreover, the electrical properties of CNT can be modified via functionalization processes, reflected as an increased electrical conductivity [9,26,27] and low resistance during charge transfer in aqueous and non-aqueous solutions [21]. Such properties are important in electrochemical measurements, which depend directly on an intermolecular electronic transfer process between the electroactive species and the electrode when a potential difference is applied.

The activity of CNT can be further improved by chemical mixed interaction with both organic molecules and biomolecules (polysaccharides and proteins) [28]. At this respect, CNT doped with chitosan have been reported in various investigations due to the excellent results obtained in the modification of glassy carbon electrodes (GCE), primarily in bioelectrochemistry [18, 29-34] and environmental remediation [35]. The functionalization of MWCNTs in HNO_3 allows the insertion of carboxyl and hydroxyl groups [23,36], which facilitates interactions with the chitosan amino and hydroxyl groups by hydrogen bonds. The possible interactions between Cd(II) and chitosan ions are

shown in Fig. 1. It has been reported that the cadmium ion can easily complex with the amino group (-NH_2) due to the high affinity of the N-Cd bond [37].

In this work, a new voltammetric application is introduced based on a glassy carbon electrode (GCE) modified with MWCNTs-chitosan (MWCNTs-Chit) for the quantification of trace levels of Cd(II) in aqueous solution. The MWCNTs-Chit/GCE was characterized by various electrochemical techniques, and the morphology was analyzed by scanning electron microscopy (SEM). To evaluate the efficiency of this electrode in quantifying cadmium by SWV, an analytical validation was performed, and an interference study was conducted to assess its application in real water samples.

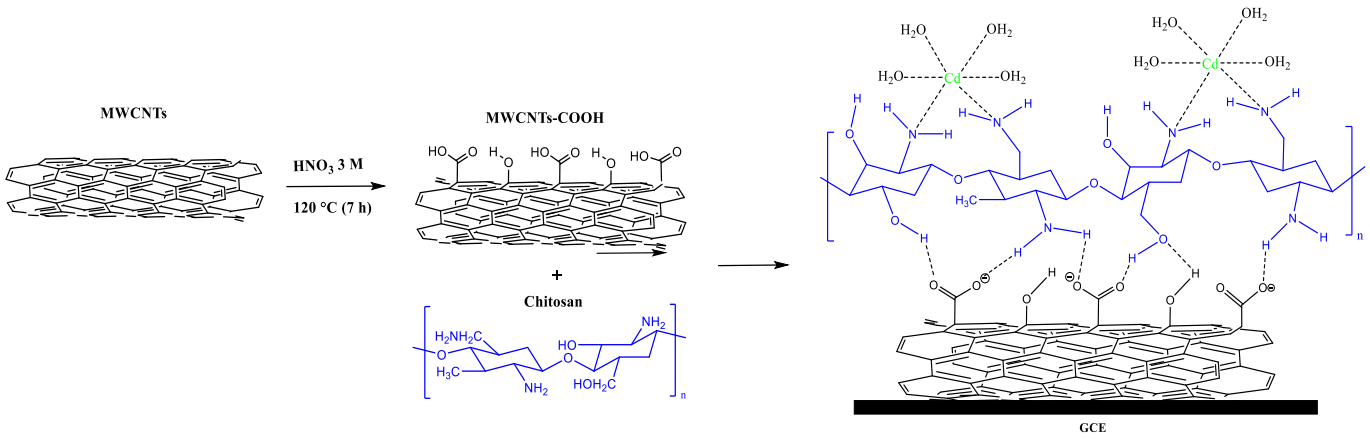

Figure 1. Scheme of the chemical modification of electrode with MWCNTs-Chit and supramolecular interaction between chitosan and MWCNTs complexing Cd(II) ions.

2. EXPERIMENTAL METHOD

2.1. Materials

All chemical reagents used were analytical grade and of the highest purity. A standard solution of Cd(II) 100 mg L^{-1} from Merck (Germany) was used. The supporting electrolyte was a 0.1 M acetate buffer prepared with CH_3COOH (99%) and CH_3COONa (99%) from Sigma-Aldrich. Dilutions were prepared with ultrapure deionized water (18 MΩ cm). For the parameters optimization, NaCl (99%), HNO_3 (70%), HCl (37%), $K_3[Fe(CN)_6]$ (99%) and KCl (99%) from Sigma-Aldrich were used. The interference study comprises utilization of $CoCl_2$ (99%), $Pb(NO_3)_2$ (98%) and $HgCl_2$ (98%) from J. T. Baker.

2.2. Functionalization and purification of multilayer carbon nanotubes (MWCNTs)

0.5 g MWCNTs (≥98% carbon basis; OD x ID x L = 10 nm ± 1 nm x 4.5 nm ± 0.5 x 3~6 µm, as determined by transmission electron microscopy (TEM) was weighed. The MWCNTs were heated at 270°C for 60 min to eliminate impurities. Subsequently, a chemical digestion was performed in 3 M HNO_3 by continuous reflux during 7 h at 120 °C. The samples were then filtered (Whatman filter No. 2)

and washed with deionized water, dried in an oven during 1 h at 35°C, and stored in a desiccator until use [38].

2.3. Electrode modification with MWCNTs-Chit

In this step, 10 mL of 0.5% chitosan (Sigma-Aldrich) was prepared in 2 M CH_3COOH, and the solution was ultrasonically dispersed (Chicago Electronic®) during 30 min. Subsequently, 25 mg functionalized MWCNTs was added to the chitosan solution and homogenized with a magnetic stirrer for 45 min. Then, 5 µL was added to the surface of the GCE (Φ = 3 mm), which had been previously polished with alumina powder (0.3 µm). The electrode was allowed to dry until a uniform dispersion was observed. The sample was then immersed in 0.1 M NaOH solution during 5 min to remove traces of CH_3COOH and it was rinsed with deionized water and 10 mL of ethanol (99%, J. T. Baker). Finally, the electrode was allowed to dry and was used immediately for experimentation.

2.4 Instrumentation

All experiments were carried out in an electrochemical cell with a three-electrode arrangement. A saturated calomel electrode (SCE) was employed as a reference electrode, and a platinum mesh was used as the auxiliary electrode. Cyclic voltammetry (CV), electrochemical impedance spectroscopy (EIS), and SWASV were performed using a VSP-300 potentiostat/galvanostat (Bio-Logic Science Instruments) with the software EC-Lab® V.10.32. The pH was adjusted via the addition of standard solutions of 0.1 M NaOH and 0.1 M HCl using a Thermo Scientific Orion 3 StarTM pHmeter. All experiments were performed at room temperature (25°C ± 2°C).

2.5. Morphological characterization of the MWCNTs-Chit electrode

Micrographs of the surface morphology of the modified electrode were obtained by SEM, and the elemental composition was analyzed by X-ray energy dispersion spectrometry (EDS) using a JEOL JSM-7000F electron microscope.

2.6. Analytical procedure

Measurements of Cd(II) solutions were performed in a 0.1 M acetate buffer at pH 5 (supporting electrolyte). No oxygen purge was performed to simulate real-time analysis conditions. The modified electrode (MWCNTs-Chit/CGE) was used as a working electrode, and peak currents of Cd(II) ion samples with known concentrations were measured. The electroanalysis began at a potential of -1.0 V *vs.* SCE and continued for 60 s (deposition time) or until analyte accumulated on the electrode surface. SWASV was then performed, and the peak current was recorded at -0.80 V *vs.* SCE, corresponding to the Cd(II) peak potential, with the following parameters: pulse height (E_{SW}) of 25 mV, frequency (f) of 100 Hz, and step height (E_{step}) of 5 mV. EIS was performed in a frequency range of 100 kHz to 0.01 Hz

with a ±10 mV peak-to-peak amplitude *vs.* the open circuit potential (OCP) over a duration of 10 min.

3. RESULTS AND DISCUSSION

3.1 Morphological analysis by SEM

The morphology of the glassy carbon electrodes modified with MWCNTs and MWCNTs-Chit were characterized by SEM. Fig. 2 shows three micrographs of different surfaces. For the unmodified glassy carbon (Fig. 2a), a relatively flat, smooth surface was observed. As shown in Fig. 2b, the MWCNTs were distributed in a highly disorganized manner. This micrograph has a low definition due to the formation of lumps and agglomerations, suggesting that a lower CNT concentration should be used. As shown in Fig. 2c, the MWCNTs exhibit a more even dispersion when they are attached to chitosan, which provides a greater electrode area for interaction with Cd(II) ions. This phenomenon may be due to supramolecular interactions (MWCNTs-chitosan), where the chitosan, which is anchored by hydrogen bonds, can protect and stabilize the CNT, thus preventing a wrinkled and tangled structure, as observed in the CNT-modified electrode without chitosan.

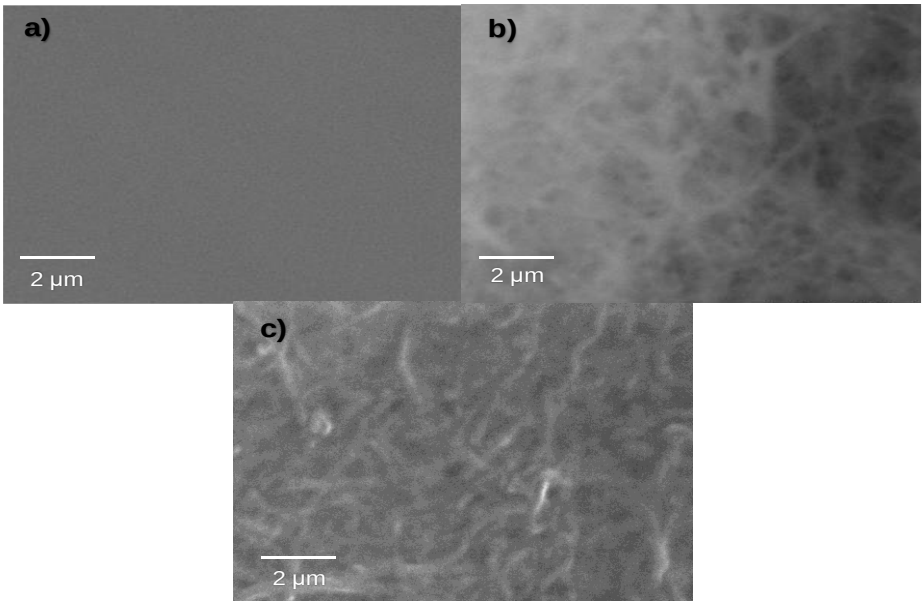

Figure 2. SEM images of electrodes a) GCE, b) MWCNT/GCE, c) MWCNTs-Chit/GCE.

3.2 Electrochemical impedance spectroscopy (EIS)

EIS is one of the most effective techniques for characterizing electrochemical processes on an electrode/dissolution interface. The Nyquist diagram is a typical representation of an impedance spectrum, and the charge transfer resistance (R_{ct}) provides information regarding the kinetics of the process [39]. Thus, EIS was used to evaluate the properties of the MWCNT/Chit-modified electrode in 1 mM $[Fe(CN)_6]^{3-}$ + 0.1 M KCl.

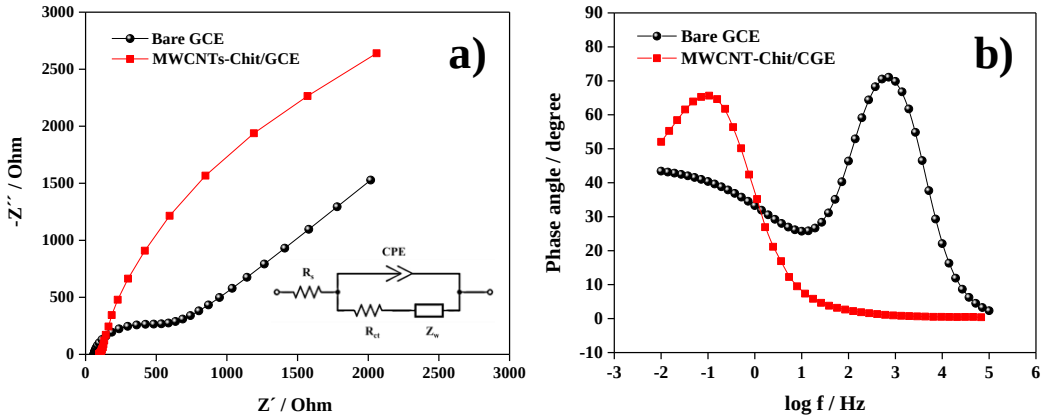

Figure 3. Impedance results for different conditions of superficial modification of GCE a) Nyquist diagram (inside Randles circuit) b) Phase angle diagram.

Charge transfer resistance (R_{ct}) and double-layer capacitance (C_{dl}) parameters were determined by simulating the experimental results using Randles circuit as an equivalent circuit, as shown in Fig. 3a, where the resistance of the electrolyte solution (R_s) is in series with a parallel combination of the charge transfer resistance (R_{ct}) and Warbug impedance (Z_W). Due to the physical properties of MWCTNs (roughness, porosity, high surface area, among others), a constant phase element (CPE) was used as the CPE and is closely related to the distribution of "unbalanced" current due to the surface defects [38,40]. According to equation 1, the CPE is an element that describes the dielectric properties whose impedance response is based on the angular frequency (ω), however, the phase angle is not time-based.

$$Z_{CPE} = \frac{1}{Y_0(j\omega)^n} \quad (1)$$

Y_0 it is a constant, while j and ω are given by $j = \sqrt{-1}$; $\omega = 2\pi f$. The effect of the accumulation or repulsion of electrical charges on the interface is described with the value of n ($-1 \leq n \leq 1$). If n=1, the surface acts as an ideal capacitor and Y_0 will be equal to the capacitance value according to $C = Y_0(\omega)^{n-1}$ [41]. The Nyquist diagram shown in Fig. 3a indicates that R_{ct} decreases for the MWCNTs-Chit/GCE in contrast to the GCE bare. Table 1 presents the values obtained for each electrode condition standardized with respect to the area, and section 3.3 shows the procedure for calculating the MWCNTs-Chit/GCE area. The R_{ct} values decreased by a factor of eight approximately, and a significant increase in CPE was recorded for the GCE. This result is attributed to the increased superficial area and the accumulation of surface charges. Similar results were reported by Galicia et al. [38] under static conditions and laminar flow.

Table 1. Impedance parameters of each electrode condition, using the equivalent Randles circuit.

Electrode	EIS parameters					
	R_s (Ω cm^2)	CPE (F s^{n-1} cm^{-2})	n	R_{ct} (Ω cm^2)	W	χ^2
Bare GCE	1.1±0.03	$0.22\times10^{-4}\pm0.5\times10^{-6}$	0.91	34.3±0.6	812.9±8.4	2.6×10^{-4}
MWCNT-Chit/GC	8.7±0.1	$1.78\times10^{-4}\pm1.1\times10^{-6}$	0.93	2.1±0.1	1386.5±13.1	7.9×10^{-4}

These results suggest that by modifying the electrode surface with MWCNT-Chit, the kinetics of the redox processes are strongly accelerated at the interface. It has been shown that the maximum phase angle (φ) can be used as a parameter to determine the electronic transfer kinetics, because φ is related to R_{ct} and R_s (Eq. 2), the phase angle decreases when the charge transfer occurs more rapidly at the electrode interface [42, 43].

$$\varphi = \tan^{-1}\left(\frac{1}{1 + 2R_{ct}R_s}\right) \quad (2)$$

As shown in Fig. 3b, a smaller phase angle was observed for the modified electrode (φ = 65), compared with the unmodified electrode (φ = 71), indicating that the kinetics are faster on the modified surface. To confirm this interpretation, the standard rate constant (k_{app}) was determined, considering the typical redox reaction in aqueous medium as a reference: $[Fe(CN)_6]^{3-} \leftrightarrow [Fe(CN)_6]^{4-}$. The constant was calculated according to the following equation (Eq. 3).

$$R_{ct} = \frac{RT}{(nF)^2 A C k_{app}} \quad (3)$$

where A is the electrode area (cm^2), n is the number of electrons (n = 1), R is the ideal gas constant (8.314 J mol^{-1} K^{-1}), T is the absolute temperature (K), C is the analyte concentration (mol cm^{-3}), and F is the Faraday constant (96,485 C mol^{-1}) [44]. The standard rate constants were 0.13 cm s^{-1} and $7.8x10^{-3}$ cm s^{-1} for the MWCNT-Chit/GCE and bare GCE samples, respectively. These results confirmed that the redox reaction occurs more rapidly in the presence of MWCNT-Chit, as previously observed in impedance experiments. It is important to note that although the MWCNT-Chit/GCE area is larger, the kinetics of the redox process are still more favorable, considering that the area and the k_{app} are inversely proportional. This behavior is primarily attributed to the electrical and electronic properties of MWCNT, which are better for electron transfer than glassy carbon. In addition, the increased surface area facilitates diffusion during the redox processes of $[Fe(CN)6]^{3-/4-}$ at the interface.

3.3. Voltammetry characterization

By means of CV, the effective work area was determined using the de Randles–Sevcik equation (Eq. 4) by analyzing the reversible process of $[Fe(CN)_6]^{3-}$.

$$i_p = 0.4463\left(\frac{F^3}{RT}\right)^{1/2} n^{3/2} A C v^{1/2} D^{1/2} \quad (4)$$

The peak current was measured at 10, 20, 50, 100, 200 and 500 mV s^{-1}. Subsequently, the area was calculated using the following parameters: the number of electrons transferred (n = 1), the diffusion coefficient of $[Fe(CN)_6]^{3-}$ ($7.6x10^{-6}$ cm^2 s^{-1} [45]), and the $[Fe(CN)_6]^{3-}$ concentration ($1x10^{-6}$ mol cm^{-3}). The peak current (ip_a) was measured in μA, and the scan rate (v) was given in V s^{-1}. As shown in Fig. 4, there is a linear correlation between ip_a and $v^{1/2}$, indicating that the mass transport mechanism at the

interface is controlled by diffusion. This finding was confirmed by the log-log graph of ip_a *vs.* v, as shown inside of Fig. 4, which has a slope close to 0.5 [46]. From the slope fitted to ip_a *vs.* $v^{1/2}$, the effective work area was found to be 0.5932 cm^2. This increase in the area is consistent with the results obtained by EIS, exhibiting an increase in C_{dl}. This result can be primarily attributed to the larger surface area of MWCNT-Chit, which has both a large surface area and a large molecular size [28].

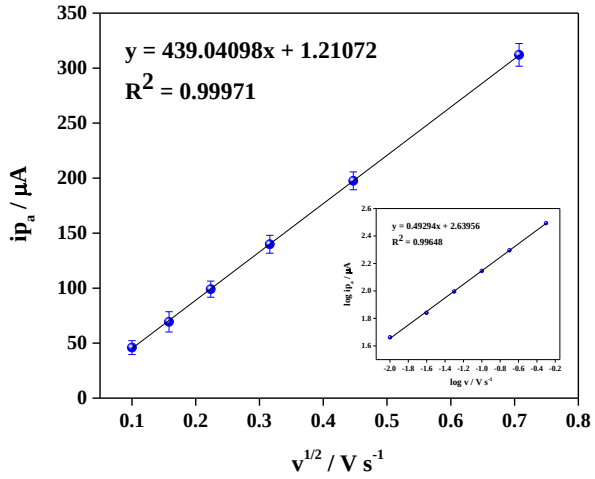

Figure 4. Graph of ip_a vs. $v^{1/2}$, at different scan rates with 1 mM $[Fe(CN)_6]^{-3}$ + 0.1 M KCl. Zoom: Graph of log Ip_a *vs.* log v.

Using SWASV technique, the Cd(II) detection efficiency was investigated using the MWCNTs-Chit/GCE. The modified electrode was initially evaluated in a solution of 30 µg L^{-1} Cd(II) in 0.1 M HCl, with standard SWASV parameters of E_{step} = 25 mV, E_{SW} = 5 mV, calculated E_{step} = 50/n, and E_{SW} = 10/n, where n is the number of transferred electrons [14,15]. Figure 5 presents voltammograms of electrodes with and without the modification. A well-defined peak corresponding to the electrochemical oxidation of Cd(II) was observed at -0.8 V *vs.* SCE for MWCNTs-Chit/GCE. For the bare GC electrode, only instrumental noise was observed, demonstrating the need to modify the glassy carbon electrode in order to detect species at a lower concentration.

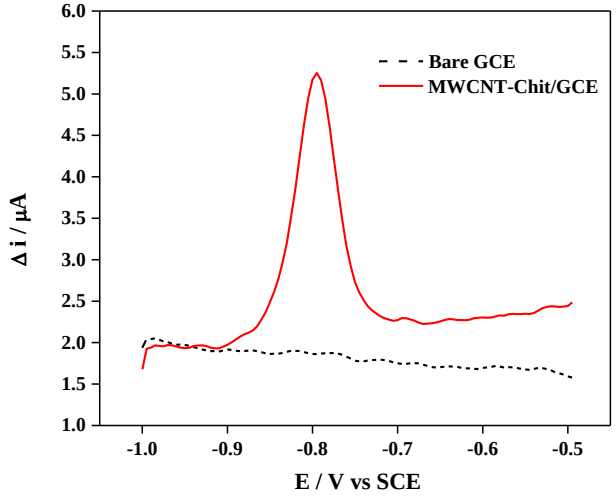

Figure 5. SWASV of 30 µg L^{-1} Cd(II) in 0.1 M HCl. E_{SW}: 25 mV, f: 100 Hz.

3.4. Optimization of experimental parameters

The influence of SWASV parameters was studied in order to optimize the experimental conditions, which impact the quality of the Cd(II) quantification. The effect of the supporting electrolyte was studied in different media: HCl, NaCl, HNO_3, and acetate buffer in a 0.1 M concentration.

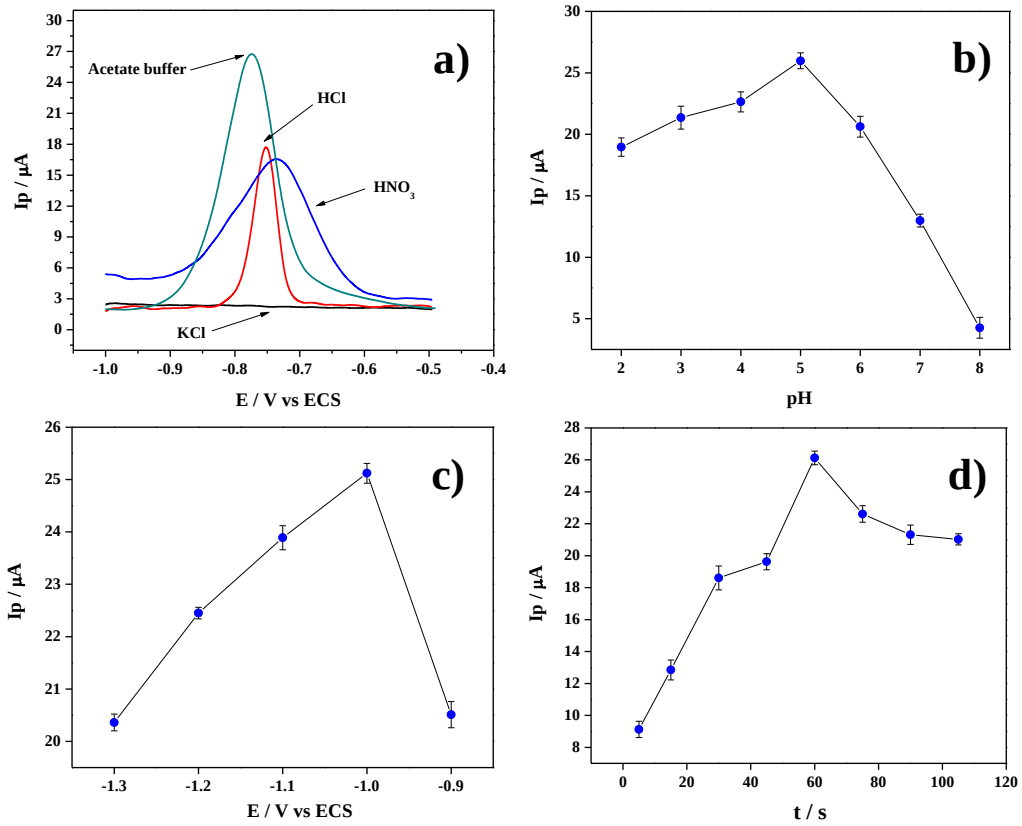

Figure 6. Optimization of SWASV parameters in 30 µg L^{-1} Cd(II) with a MWCNT-Chit/GCE: a) electrolyte effect b) influence of pH c) effect of deposition potential d) effect of the time of deposition.

As depicted in Fig. 6a, the highest current was recorded in the 0.1 M buffer solution; thus, this electrolyte was selected for subsequent experiments. The influence of pH was studied over a range of 2–8, as shown in Fig. 6b. The highest current was observed at a pH of 5. This result is attributed to the fact that at lower pH values, the chitosan amino groups protonate, weakening the interactions with Cd(II) ions by electrostatic repulsion; in contrast, at higher pH values, the Cd(II) ions may precipitate as hydroxides [47]. The deposition potential was studied over a range of -1.3 to -0.9 V *vs.* SCE. The highest recorded current was obtained at a potential of -1 V *vs.* SCE, as shown in Fig. 6c. At more positive potentials, the current declined significantly. The second highest current value was recorded at -1.1 V *vs.* SCE; however, at this potential and at more negative potentials, small bubbles appeared in the electrode, corresponding to the electrochemical reduction of H^+ ions evolving into hydrogen gas. In addition, highly cathodic potentials could not be scanned because the electroactivity window (not shown)

ends at approximately 1.25 V *vs.* SCE. The occurrence of an electrochemical reaction may cause the peak current, i_p to decrease at more negative potentials because hydrogen bubbles interfere with the deposition of metal at the interface reducing the amount of the deposited Cd(II) consequently reducing the kinetics of the process. This effect has been reported by Ezzahra et al. [39], Afkhami et al. [43], and Dahaghin et al. [47]. The effect of deposition time was investigated over a range of 5–100 s. As illustrated in Fig. 6d, an increase in the peak current was initially recorded up to 60 s, followed by a gradual decrease. Therefore, this deposition time of 60 s was applied for the following experiments.

3.5 Calibration curve

To verify the correlation between peak current and concentration, a calibration curve was constructed under optimal conditions for a Cd(II) concentration range of 1–50 µg L^{-1} in a 0.1 M acetate buffer at pH 5 with a deposition time of 60 s, as displayed in Fig. 7. The following linear equation was determined: $i_{p(\mu A)} = 0.67696C_{Cd(II)} + 6.19482$ with a correlation coefficient of 0.9991.

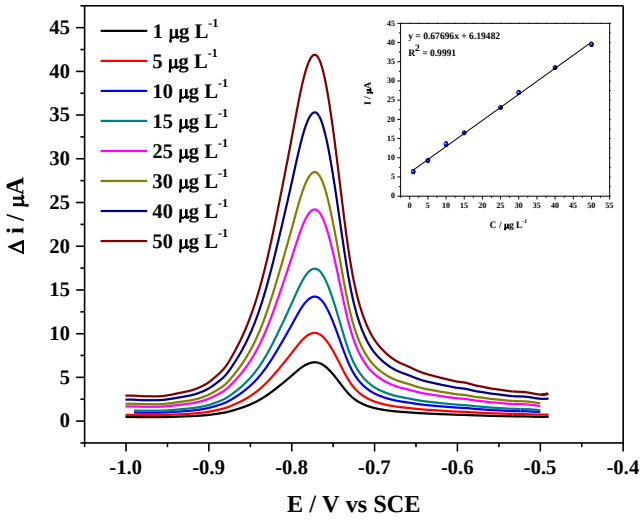

Figure 7. SWV for different concentrations of Cd(II), in an 0.1 M acetate buffer at pH 5, modified glassy carbon (Φ=3 mm), with MWCNT-Chit, E_{SW}: 25 mV, *f*: 100 Hz. (inside calibration curve).

The limit of detection (LOD, 3σ/m) and quantification (LOQ, 10σ/m) were calculated and compared to values reported in the literature [47], where σ is the standard deviation of the blank solution (0.1 M acetate buffer at pH 5) with n = 25 and m is the slope of the linear equation. The LOD and LOC values were 0.089 µg L^{-1} and 0.2966 µg L^{-1}, respectively. Table 2 presents a comparison of these results with respect to other proposed methods.

Table 2. Compilation of techniques and data applied for detection of Cd(II) in aqueous systems.

Electrode	Method	Lineal range	Detection limit	Ref
MWCNT-Chit/CGE	SWASV (Square Wave Anodic Stripping Voltammetry)	1 – 50 μg L^{-1}	0.09 μg L^{-1}	This work
MWCNT/GCE	ASV (Anodic Stripping Voltammetry)	$1x10^{-5}$ - $2.5x10^{-8}$ M	$6.0x10^{-9}$ M	[46]
MWCNT-EBP-NA/GCE	SWASV	1 – 50 μg L^{-1}	0.06 μg L^{-1}	[23]
L-MWCNT/CPE_{IL}	ASV	0.2 – 23 μg L^{-1}	0.08 μg L^{-1}	[43]
MWCNT-Nafion/GCE (mercury film)	DPASV (Differential Pulse Anodic Stripping Voltammetry)	10 – 250 μg L^{-1}	25 ng L^{-1}	[49]
NGP-Nafion/GCE (mercury film)	DPASV	0.25 – 5 μg L^{-1}	3.5 ng L^{-1}	[49]
SO/GCE	AdSV (Adsorptive Stripping Voltammetry	$1x10^{-8}$ - $1x10^{-10}$ M	3.30×10^{-11} M	[50]
Sb/NaMM-CPE	ASV	4 – 150 μg L^{-1}	0.25 μg L^{-1}	[51]

3.6. Validation of the analytical method

To validate the applicability of MWCNTs-Chit/GCE for Cd(II) quantification, several samples of tap water and drinking water were analyzed using the standard addition method. No pre-concentration treatment was applied to the collected water samples; the pH was simply adjusted to 5, and the measurements were performed in a buffer solution of 0.1 M acetate. As shown in Table 3, the actual concentrations of Cd(II) in the tap and drinking water samples could not be quantified because the ion concentrations were below the LOD for this method. The percentage recovery (%R) values in the water samples were found within the ideal range (100 ± 2%), and the relative standard deviation (%RSD) was less than 5%, demonstrating the excellent precision and accuracy of the modified electrode. Thus, the MWCNTs-Chit/CGE is a viable tool for the analysis of real samples.

Table 3. Recovery data for detection of Cd(II) in drinking and tap water using MWCNTs-Chit/CGE in 0.1 M acetate buffer (pH 5).

Sample (Cd^{2+})	Original (μg L^{-1})	Added (μg L^{-1})	Found (μg L^{-1})	Recovery (%)	RSD (%)
Drinking water 1	ND	5	5.01	101.97	2.99
Drinking water 2	ND	10	9.81	98.07	2.14
Tap water 1	ND	5	4.95	99.09	3.16
Tap water 2	ND	10	9.85	98.52	3.98

ND: Not detected, n = 10.

3.7. Selectivity

The selectivity of the MWCNTs-Chit/GCE was investigated in a solution containing Cd(II) ions.

Besides, another ion species were added during the pre-concentration period. Pb(II) and Co(II) were added at concentrations of 30 µg L^{-1}, while Hg(II) was added at 100 µg L^{-1}. Figure 8 exhibits four characteristic signals corresponding to the anodic peaks of the ionic species. These oxidation peak potentials do not overlap with the specific oxidation peak for cadmium detection. Therefore, the accuracy and precision of this detection remained constant, with only a slight shift towards -0.7 V *vs.* SCE. It is important to note the clear separation between the Cd(II) and Pb(II) peaks, whose peak potentials are very close, demonstrating the high accuracy of our modified electrode. In addition, Co(II) and Hg(II) ions were clearly detected, indicating that our modified electrode has potential for simultaneous detection of these species.

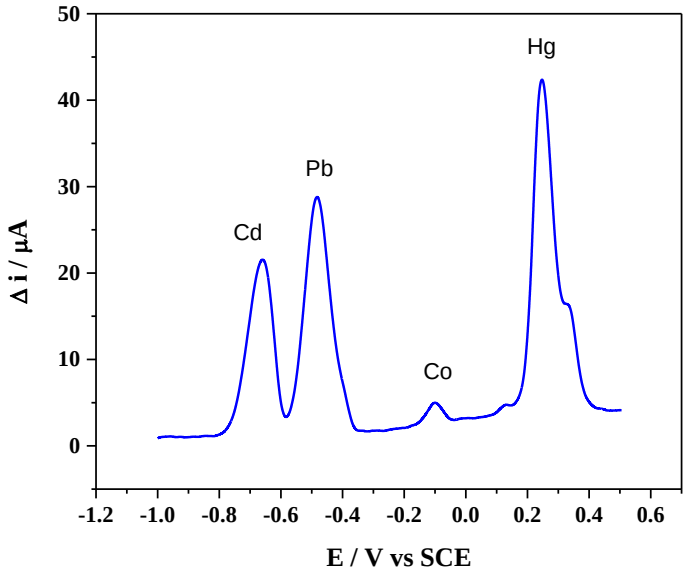

Figure 8. Results for selectivity-interference test in presence of 30 µg L^{-1} Cd(II), 30 µg L^{-1} Pb(II), 30 µg L^{-1} Co(II) and 100 µg L^{-1} Hg(II), using SWASV with MWCNTs-Chit/GCE. E_{SW}: 25 mV, *f*: 100 Hz.

4. CONCLUSIONS

This paper reports on a highly sensitive and accurate electrochemical method for detecting cadmium(II) in aqueous solution. Nanostructured modified glassy carbon electrodes with a scaffold of MWCNT and chitosan biopolymer were successfully assembled for application with SWASV. Impedance analysis verified an enhancement in the charge transfer efficiency for this modified electrode. This enhancement was characterized by CV and EIS analysis, and the parameters for electrochemical detection via SWASV were optimized. An acetate buffer was employed as the electrolyte for our experiments. Further experiments for real systems of both drinking water and tap water exhibited excellent accuracy and precision for the MWCNTs-Chit/GCE. Finally, this modified electrode exhibited high efficacy, with a promising sensibility and selectivity in the presence of several ionic toxic heavy metals, including Pb, Co, and Hg.

ACKNOWLEDGEMENTS
Authors want to thank M. C. Hortensia Reyes Blas in the Advanced Microscopy Laboratory of Engineering and Technology Institute (IIT-UACJ) by his technical assistance for obtaining SEM images.

References

1. M. Lin, M. Cho, W. S. Choe, Y. Son and Y. Lee, *Electrochim. Acta*, 54 (2009) 7012.
2. Z. Koudelkova, T. Syrovy, P. Ambrozova, Z. Moravec, L. Kubac, D. Hynek, L. Richtera and V. Adam, *Sensors*, 17 (2017) 1832.
3. Z. Arbab, M. Chamsaz, A. Youssefi and M. Aliakbari, *Anal. Chim. Acta*, 546 (2005) 126.
4. T. Lanez, A. Rebiai, M. Saha, M. Alia, *Int. J. Toxicol. Appl. Pharm.*, 1 (2011) 21.
5. M. Ghanei and M. Taher, *Chem. Eng. J.*, 327 (2017) 135.
6. E. Mojica, M. Vidal, B. Pelegrina and L. Micor, *J. Appl. Sci*., 7 (2017) 1286.
7. M. Gholivand and N. Karimian, *Sens. Actuators B: Chem.*, 215 (2015) 471.
8. R. Xie, L. Zhou, C. Lan, F. Fan, R. Xie, H. Tan, T. Xie and L. Zhao, *R. Soc. Open Sci.*, 5 (2018) 1.
9. S. Tursynbolat, Y. Bakytkarim, J. Huang and L. Wang, *J. Pharm. Anal.*, 8 (2018) 124.
10. T. Kazak and M. Revenko, *J. Anal. Chem.*, 64 (2009) 181.
11. M. El Mhammedi, M. Achak, R. Najih, M. Bakasse and A. Chtaini, Mater. *Chem. Phys.*, 115 (2009) 567.
12. M. El Mhammedi, M. Achak, M. Hbid, M. Bakasse, T. Hbid, A. Chtaini, *J. Hazard. Mater.*, 170 (2009) 592.
13. E. Mehmeti, M. Stankovié, A. Ortner, J. Zavansnik and K. Kalcher, *Food Anal. Methods*, 10 (2017) 3747.
14. L. Chen, C. Barus and V. Garçon, *Electroanalysis*, 29 (2017) 2882.
15. A, Bard and L. Faulkner, Electrochemical Methods: Fundamentals and Applications 2nd ed., Harris, D., (2001), United States.
16. A. Oliveira, L. Ferreira, D. Vieira, M. Meneghetti and F. Caxico, *J. Anal. Methods Chem.* 16 (2016) 1.
17. T. Mayumi, P. de Oliveira, E. Pissinati, A. Sálvio, L. Marcolino and M. Bergamini, *Bioresour. Technol.*, 143 (2013) 40.
18. M. Bueno, M. Marín, A. Contento and A. Ríos, *Food Chem.*, 192 (2016) 343.
19. S. Iijima and T. Ichihashi, *Nature,* 363 (1993) 603.
20. M. Krüger, R. Buitelaar, T. Nussbaumer and C. Schönenberger, *Appl. Phys. Letters*, 78 (2000) 1291.
21. T. Oliveira and S. Morais, *Appl. Sci.*, 8 (2018) 1925.
22. Z. Abdul, N. Azah, S. Aniq, F. Mohammad, M. Ismahadi and N. Daud, *Materials*, 11 (2018) 1902.
23. K. Balasubramanian and M. Burghard, *Small*, 1 (2005) 180.
24. G. Zhao, Y. Yin, H. Wang, G. Liu and Z. Wang, *Electrochim. Acta*, 220 (2016) 267.
25. H. Zhao, Y. Jiang, Y. Ma, Z. Wu, Q. Cao, Y. He, X. Li and Z. Yuan, *Electrochim. Acta*, 55 (2010) 2518.
26. A. Dettlaff, R. Das, L. Komsiyska, O. Osters, J. Luczak and Z. Wilamowska, *Synth. Met.*, 244 (2018) 80.
27. F. Aboufazeli, L. Reza, O. Sadeghi, M. Karimi and E. Najafi, *J. AOAC Int.*, 97 (2012) 173.
28. N. Kittana, M. Assali, H. Abu-Rass, S. Lutz, R. Hindawi, L. Ghannam, M. Zakarneh and A. Mousa, *Int. J. Nanomed.*, 13 (2018) 7195.
29. S. Mallakpour and M. Madani*, High Perform. Polym*., 27 (2014) 793.
30. P. Arias, N. Ferreyra, G. A. Rivas and S. Bollo, *J. Electroanal. Chem.*, 634 (2009) 123
31. M. Zhang, A. Smith and W. Gorski, *Anal. Chem.*, 76 (2004) 5045.
32. D. Wan, S. Yuan, G. L. Li, G. Neoh and E. Kang, Appl. Mater. *Interfaces*, 2 (2010) 3083.

33. C. Caoduro, E. Hervouet, C. Girand, T. Gharbi, H. Boulahdour, R. Delage and M. Pudlo, *Acta Biomater.*, 49 (2017) 36.
34. A. Mariño, Y. Leiva, K. Bolaños, O. Garcia and E. Nagles, *J. Electroanal. Chem.*, 30 (2015) 153
35. R. Khakpour and H. Tahermansouri, *Int. J. Biol. Macromol*., 109 (2018) 598.
36. V. Castro, B. Costa, M. Lopes, R. Lavall, K. Figueiredo and G. Silva, *J. Braz. Chem. Soc.*, 28 (2017) 1158.
37. P. Taneja, V. Manjuladevi, K. K. Gupta and R. K. Gupta. *Sens. Actuators B: Chem.*, 268 (2018) 144.
38. M. Galicia, X. Li and H. Castaneda, *J. Electrochem. Soc.*, 161 (2014) 751.
39. F. Ezzahra, A. Ouarzane and M. El Rhazi, *Arabian J. Chem.*, 10 (2017) 596.
40. M. Metikos, A. Kwokal and J. Piljac, *Biomaterials,* 24 (2003) 3765.
41. V. M. Cortez, C. Aguilar, A. Muci, A. L. Marie and M. J. Ribeiro, *Mater. Res.,* 20 (2017) 436.
42. G. Gold, D. Nkosi, K. Pillay and O. Arotiba. *Sensing Bio-Sensing Res.*, 10 (2016) 27.
43. A. Afkhami, H. Khoshsafar, H. Bagheri and T. Madrakian. *Mater. Sci. Eng. C*, 35 (2014) 8.
44. Y. Oztekin, Z. Yazicigil, A. Ramanaviciene and A. Ramanavicius, *Sens. Actuators B: Chem.*, 152 (2011) 37.
45. Y. Song, Z. Xu, X. Yu, X. Shi, H. Jiang, X. Li, Y. Kong, Q. Xu and J. Chen, *Molecules*, 22 (2017) 797.
46. D. Pamuk, I. Hüdai, A. Ece, E. Canel and E. Kilic, *J. Braz. Chem. Soc.*, 24 (2013) 1276.
47. Z. Dahaghin, A. Kilmartin, and M. Zavvar, *J. Electroanal. Chem.*, 810 (2018) 185.
48. K. Wu, S. Hu, J. Fei and W. Bai, *Anal. Chim. Acta*, 489 (2003) 215.
49. L. Wu, X. Fu, H. Liu, J. Li and Y. Song, *Anal. Chim. Acta*, 851 (2014) 43.
50. V. Kumar, M. Lütfi, N. Atar, A. Osman, L. Uzun and Z. Üstündag, *Electrochim. Acta*, 105 (2013) 149.
51. G. Chen, X. Hao, B. Lin, H. Qun and N. Bing, *Sens. Actuators B: Chem.*, 237 (2016) 570.